Anal Bioanal Chem (2006) 384: 180–190
DOI 10.1007/s00216-005-0196-1

ORIGINAL PAPER

R. E. Kunz · K. Cottier

Optimizing integrated optical chips for label-free (bio-)chemical sensing

Received: 26 July 2005 / Revised: 24 October 2005 / Accepted: 25 October 2005 / Published online: 3 December 2005

Abstract Label-free sensing is an important method for many (bio-)chemical applications in fields such as biotechnology, medicine, pharma, ecology and food quality control. The broad range of applications includes liquid refractive index sensing, molecule detection, and the detection of particles or cells. Integrated optics based on the use of waveguide modes offers a great potential and flexibility to tailor the sensor properties to these applications. In this paper, the results of a numerical study are presented, showing that this flexibility is founded on the many degrees of freedom that can be used for the integrated optical chip design, in contrast to other technologies such as those based on surface plasmon resonance, for which the materials' properties limit the range of choices. The applications that are explicitly considered and discussed include (1) bulk refractometry, (2) thin-layer sensing, for example biosensors monitoring molecular adsorption processes occurring within some 10 nm of the chip's surface, (3) thick-layer sensing with processes involving molecules or ions to be monitored within a sensing matrix extending to some 100 nm from the chip's surface, for example hydrogel-based layers and chemo-optically sensitive membranes, and (4) particle sensing with particles or, for example, biological cells to be monitored within probe volumes extending to some 1,000 nm from the chip's surface. The peculiarities for the different types of applications will be discussed, and suitable modeling methods presented. Finally, the application-specific design guidelines supplied will enable the optimization of various types of integrated optical sensors, including interferometers and grating-based sensors.

R. E. Kunz (✉)
Centre Suisse d'Electronique et de Microtechnique SA (CSEM),
Jaquet-Droz 1,
2007 Neuchâtel, Switzerland
e-mail: rino.kunz@csem.ch

K. Cottier
Optrel AG,
9630 Wattwil, Switzerland

Keywords Label-free sensing · (Bio-)chemical sensors · Evanescent-wave sensors · Integrated optical sensor chip · Waveguides

Introduction

Label-free sensing is an important method for many (bio-)chemical applications in fields such as biotechnology, medicine, pharma, ecology and food quality control. This contribution deals with a subclass of optical techniques, namely the so-called evanescent-wave sensing. Among these techniques, two have gained major relevance in recent years. The first one makes use of the well-known surface plasmon resonance (SPR) phenomenon (Refs. [1–3] and references therein), while the second one uses dielectric waveguides forming an integrated optical (IO) chip for creating the evanescent wave that is used to probe the target species in an analyte solution [4–40].

Sensing based on integrated optics offers many degrees of freedom for optimizing the IO chip design [9], in contrast to other technologies such as SPR where the material's (metal) properties limit the range of choices [5]. In order to fully exploit the potential of IO sensor chips for future practical applications, a detailed study of the complex relations between different waveguide configurations and their respective suitability for various applications is needed. The applications considered here include liquid refractive index sensing, molecule detection at the surface and in a sensing matrix, as well as the detection of particles or cells.

This paper gives an overview on the peculiarities of the IO approach, and presents guidelines for tailoring the properties of IO sensor chips to the type of applications envisaged. By means of an extensive numerical study, it is investigated how the IO chips can not only be designed for achieving maximum sensitivity, but also to obtain an optimum "signal-to-background ratio" in the sense of maximizing the sensitivity in a desired sensing region of interest, but minimizing it in the regions of noninterest, for example in the bulk analyte volume.

Figure 1 gives an overview of the configurations considered in this contribution. Fig. 1a depicts the basic configuration for IO sensing, which is studied in the section "Basics and bulk refractometer applications". Fig. 1b shows a sketch of the currently most relevant application involving the detection of molecular species, detailed in the section "Thin-layer sensing." The section "Thick-layer sensing" and Fig. 1c describe thick-layer sensing applications, where processes are to be monitored in a sensing matrix above the chip's surface. Finally, particle sensing applications, schematized in Fig. 1d, are considered in the section "Particle sensing." Here, the sensing region typically exceeds the thickness of one wavelength with processes to be monitored within probe volumes extending up to some microns from the chip's surface. Examples are particles, cells including bacteria in the field of "cellomics," or micro-refractometry of inhomogeneous media.

Results are derived for a single waveguiding film surrounded by additional layers and media. All configurations discussed are based on using purely dielectric materials. Results are given for a wavelength of 633 nm that is often used for experiments reported in the literature, and which is representative for the typical range of wavelengths of 300–900 nm used for practical sensors. It should be noted that although not considered here, the wavelength of light presents an additional parameter for tailoring the properties of IO sensor chips.

The emphasis is on pointing out the peculiarities for the different types of applications. Suitable modeling tools are presented and application-specific design guidelines established. All calculations are performed for planar dielectric (slab) waveguides. For those applications making use of channel guides, the data are approximations, but they are still useful to indicate the general tendencies. The results are presented in a form that renders them directly relevant for all types of dielectric waveguide sensing schemes, including grating couplers and interferometers, since the effects of the choice of waveguide configurations and parameter values are given in terms of the primary sensitivity [8] that is independent of the readout scheme chosen. The results are presented and summarized using explicitly the most relevant physical parameters and parameter ranges that correspond to the most important practical applications.

Basics and bulk refractometer applications

General basics

Figure 1a shows the basic waveguide configuration considered in this paper. It consists of a waveguiding film with refractive index n_f and a thickness h_f, of optional intermediate layers, and two infinitely extended media called substrate and cover, having refractive indices $n_s<n_f$ and $n_c<n_f$, respectively.

Through total internal reflection at the waveguiding film interfaces, light is confined and guided and only appears in discrete modes. The modes are characterized by their effective refractive index N which is directly proportional to the phase velocity of the guided wave. The notion of effective refractive index is central to sensing schemes

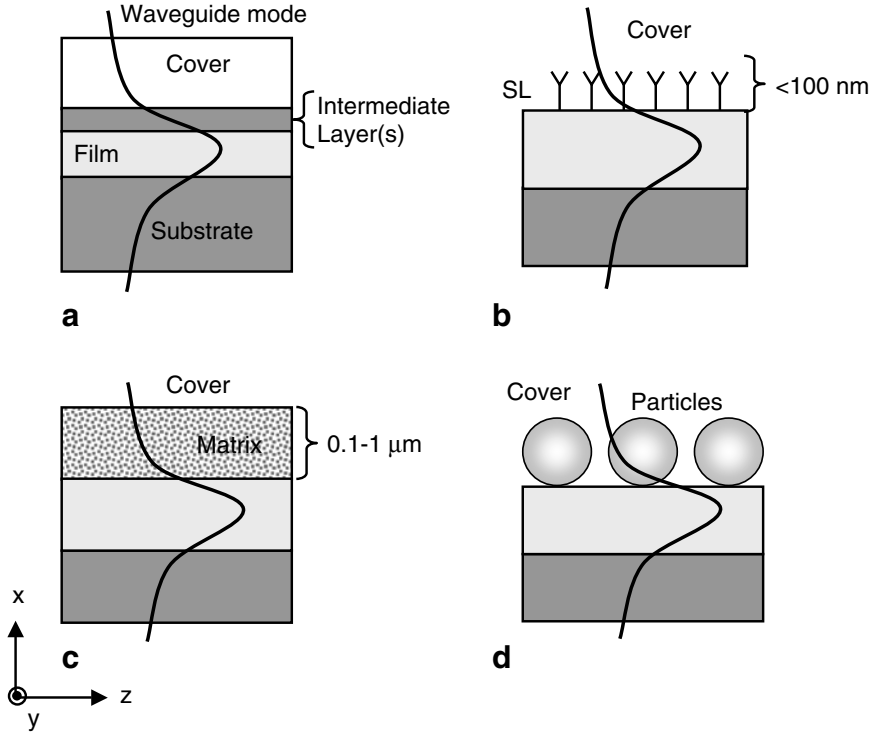

Fig. 1 **a** Basic configuration for integrated optical sensing, **b** configuration for thin-layer (*SL* sensing layer) and **c** thick-layer (*matrix*) sensing, **d** configuration for particle sensing

based on waveguides, as it is the parameter which is physically measured. It shows a functional dependence on the waveguide parameters

$$N = \mathrm{f}_N\{n_s,\ n_f,\ n_\mathrm{l},\ n_c,\ h_f,\ h_\mathrm{l},\ \lambda,\ m,\ p\}, \tag{1}$$

i.e., the refractive indices n_s, n_f, n_l, and n_c of substrate, waveguiding film, intermediate (sensing) layer, and cover medium, respectively, and the respective thicknesses h_f and h_l. The wavelength in air, the order of the waveguide mode and the polarization (TE, TM) are denoted by λ, m and p, respectively.

In the present paper, sensor sensitivities will be given in terms of changes of the effective refractive index upon changes of one or more parameters listed in the argument of the function given in Eq. (1). An outline and a short discussion on the most important parameters and waveguide configurations relevant for sensing applications, including those of the sections "Thin-layer sensing," "Thick-layer sensing," and "Particle sensing," were given in Ref. [9] (pp. 340–344).

Evanescent field penetration depth

The field penetration depth plays a crucial role for the sensing properties of an IO chip, as it defines the region inside the cover medium and near the sensor surface for which the sensor shows maximum sensitivity. In this region, the field is called evanescent, because it decays exponentially with the distance from the film interface. The field penetration depth ξ_e is defined as the distance at which the field has decayed by a factor of 1/e. It is given for the cover medium by

$$\xi_e \equiv \lambda \Big/ \left(2\pi\sqrt{(N^2 - n_\mathrm{c}^2)}\right) \tag{2}$$

as shown for instance in Ref. [17].

Figure 2 shows the variation of the penetration depth of the evanescent wave of the TM_0 mode in the cover medium as a function of the substrate refractive index n_s=1..2 and the waveguiding film thickness h_f=0..500 nm. We chose fixed values of n_c=1.33 (aqueous solutions) and n_f=2.13 (Ta_2O_5) for the film refractive index [16]. Unless other values are given explicitly, these values will also be used through the remainder of the paper.

The main conclusions which can be drawn from the results displayed in Fig. 2 are that large film thicknesses and high film refractive indices lead to a small penetration depth, and that a small substrate index n_s leads to a large penetration depth.

What is also indicated in the figure is the so-called cutoff condition, defining the region of the parameter space where guided modes (here of type TM_0) do exist at all.

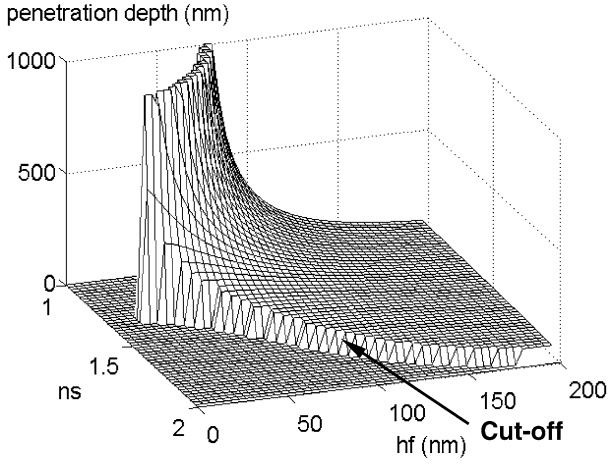

Fig. 2 Field penetration depth in the cover medium versus waveguide thickness h_f and substrate refractive index n_s

Near cutoff, the effective index N is close to the larger of the two bulk refractive indices n_s and n_c. Hence, for $n_\mathrm{s}>n_\mathrm{c}$, Eq. (2) yields the maximum penetration depth that is finite. For $n_\mathrm{s}<n_\mathrm{c}$, the penetration depth can be made arbitrarily large. The minimum values for the penetration depth are obtained for very large thicknesses h_f of the waveguiding film, where N will eventually reach the value $N \approx n_\mathrm{f}$.

As a further illustration, the detailed variation of the mode power density in a vertical direction to the waveguiding film is shown in Fig. 3 for two Ta_2O_5 waveguides with different parameters. The unit of the normalized power density is 1/microns of vertical distance.

Figure 3a is for a typical example of a configuration with a low-index substrate, enabling large penetration depths to be obtained. The main reason for the distinctly smaller penetration depth ξ_e=156 nm for the TE_0 mode than for the TM_0 mode (ξ_e=1,002 nm) is the fact that the TM_0 mode is rather close to the cutoff condition. This is not the case for the second configuration that results in quite similar values of the penetration depth of 80 and 98 nm for the TE_0 and TM_0 modes, respectively.

Other examples of mode power density profiles for TE_0 and TM_0 modes in TiO_2 waveguides were presented in Ref. [17], where also some comments on the discontinuities observed for the TM_0 modes and on "mode confinement" can be found (p. 655).

As an example of the importance of the field penetration depth in a practical application, the interested reader is referred to Ref. [5]. There, an example shows that the disturbing effect of unwanted variations of the bulk refractive index was 2–3 times smaller for IO sensors than for sensors based on SPR. It was shown that this effect mainly was due to the smaller field penetration depth in the case of the waveguide, the penetration depth for SPR sensors typically being limited to the range of about 180–230 nm for aqueous cover media with a refractive index n_c=1.33 at a wavelength of 633 nm (see Table 2 in Ref. [5]). There is a limited possibility for varying the penetration depth also for SPR sensors. However, the modifications

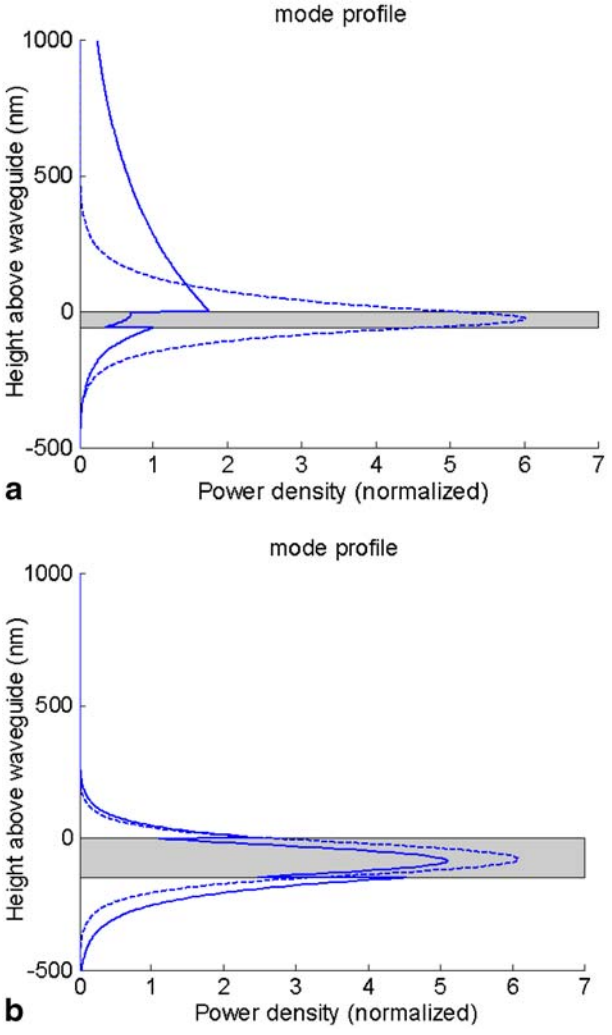

Fig. 3 Mode profiles for the TE_0 (*dashed lines*) and TM_0 (*solid lines*) modes for two different waveguides with parameter values n_s=1.2, h_f=60 nm (**a**) and n_s=1.52, h_f=150 nm (**b**)

compromise the performance for practical applications. For example, a thin dielectric layer may be deposited on top of the metal film; however, this completely changes the chemical nature of the surface, requiring a big effort in developing new assay chemistry in the case of biosensor applications.

Bulk volume refractometry

In this section, a waveguide configuration as shown in Fig. 1a is considered without any intermediate layers. The quantity to be measured (the measurand) is the refractive index n_c of the cover medium. Therefore, what is considered here are the changes of the effective index N upon changes of the refractive index of the cover (bulk) medium, expressed by the partial derivative

$$S_{bulk} \equiv \partial N / \partial n_c \,. \tag{3}$$

As pointed out in Ref. [9], IO sensing offers many powerful degrees of freedom for optimizing the properties of sensing chips towards the intended applications. One such parameter is the penetration depth ξ_e given by Eq. (2).

In order to take full advantage of the many degrees of freedom existing for designing IO sensor chips, selecting the best waveguide configurations and the most appropriate parameter values needs careful considerations. In the following, we will examine the possibilities for the special case of bulk refractometric measurements by numerical simulations of the influence of some important design parameters such as substrate refractive index and waveguiding film thickness. The results were obtained by using an in-house computer program based on solving the mode equation [17, 26].

For limiting the number of plots, we will typically show the results for the TM_0 modes only, which in general show similar behavior as the TE_0 modes, with some exceptions, such as a different cutoff condition.

The aim of this section is to present design considerations and modeling results for achieving IO sensor chips with a high sensitivity S_{bulk} as defined by Eq. (3). Fig. 4 reveals the dependence of the sensitivity on the most

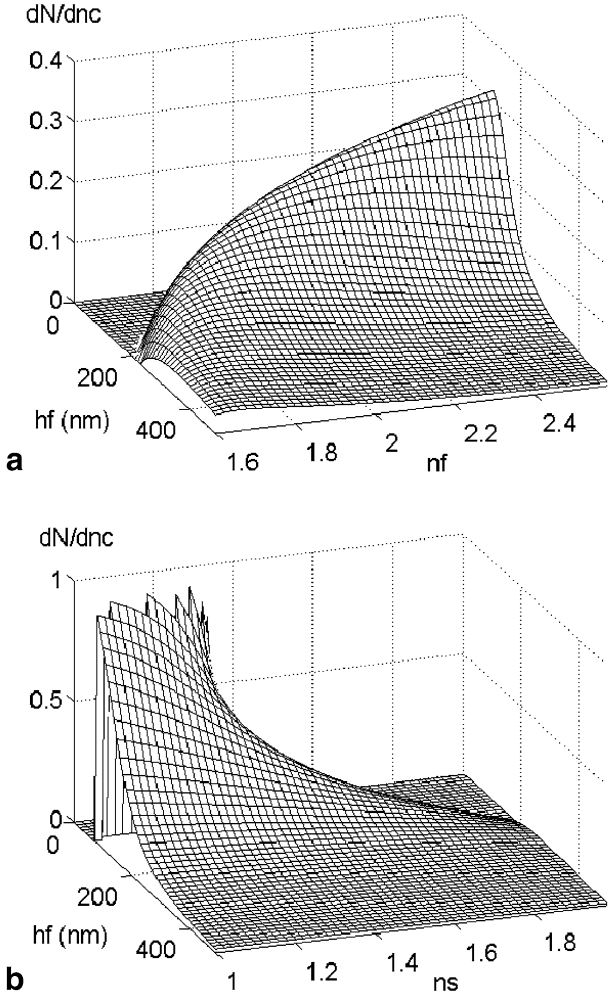

Fig. 4 Bulk volume refractometric sensitivities versus waveguide parameters h_f, n_f (**a**) and h_f, n_s (**b**) for the TM_0 mode

important parameters, i.e., the refractive indices of the waveguiding film and the substrate medium as well as the thickness of the waveguiding film.

Results are reported for the TM_0 mode only, because the type of influence is very similar for the TE_0 and the TM_0 modes. Fig. 4 shows that the film refractive index has a markedly different effect on the sensitivity than the substrate refractive index. As can be seen in the figure, small film thicknesses, large film refractive indices and small substrate refractive indices result in high sensitivities. For a given combination of n_s and n_f, the film thickness is a powerful parameter to choose (or optimize) the sensitivity.

Using these guidelines, an optimum waveguide configuration for bulk refractometry is derived in Table 1, using a high refractive index (TiO_2) film and a low refractive index substrate. Comparison of Figs. 2 and 4 gives insight into the strong relation between sensitivity and penetration depth. The important connection between this relation and the fraction of power flowing inside the cover medium was pointed out in Ref. [17].

A sensitivity enhancement by making use of a free-standing waveguiding film was reported in Ref. [20]. In this special geometry, the sensing occurred simultaneously in the cover and substrate media.

In recent publications [14, 15], configurations where the substrate refractive index is smaller than the cover refractive index ($n_s<n_c$) were termed "reverse symmetry waveguides" because most publications report on IO sensors where $n_s>n_c$. In fact, the reverse symmetry waveguide type was already used much earlier, one example being the refractometric measurement of ion-selective (optode) membranes by means of IO chips where the refractive index of the spin-coated optode membrane was larger than that of the substrate [34]. Since the membrane was much thicker than the penetration depth, this type of sensor also belongs to the "bulk sensing" type, the membrane playing the role of the cover medium. The optical properties of the real cover medium (aqueous solution) were irrelevant in this case, since no power was propagating in this region.

Despite the additional cost of lower-index substrates, however, for applications where it is crucial to achieve very large penetration depths with reasonably low fabrication tolerances, choosing low-index substrates with $n_s<n_c$ is important. One such application is the detection of micrometer-sized biological objects present in the cover medium (Refs. [15, 25] and the section "Particle sensing"). Sensor chip configurations based on using semiconductor substrates (e.g., Si) would be favorite candidates for realizing reverse symmetry waveguides, since porous SiO_2 layers could be used instead of the common thermal SiO_2 buffer layers between a thick substrate and the film. Such configurations including also other elements (light sources, detectors, modulators) integrated on the substrate have been described [9, 26–29].

Thin-layer sensing

Fundamentals

This section deals with the currently most relevant IO sensor applications involving the detection of molecular species being adsorbed to a thin recognition layer immobilized on the sensor chip's surface. This thin-layer type of applications is especially relevant for biosensors (for example in the field of proteomics) with adsorption processes occurring in a surface-sensing region within some 10 nm of the chip's surface.

The basic configuration (Fig. 1b) consists of a thin sensing layer with refractive index n_l and thickness h_l inserted between the film and cover media. This type of sensor has been described in many publications [4–13, 16, 17, 35, 36].

To work out the essentials in this section, we use the following simplified model for describing the (bio-)chemical processes occurring in the sensing layer. It is assumed that the adsorption or desorption of molecules to and from the sensing layer will result in a change of its thickness h_l only, and will not affect its refractive index, which is assumed to have a constant value n_l=1.45 [8]. Furthermore, it is assumed that the cover refractive index may vary, for example, owing to temperature fluctuations or different chemical composition, but only by a small amount around n_c=1.33 and without affecting the sensing layer refractive index.

Based on these assumptions, the thin-layer ("2D") sensitivity S_{2D} is given by the partial derivative

$$S_{2D} \equiv \partial N / \partial h_l \tag{4}$$

of the effective index N by the sensing layer thickness.

For practical applications, it is not sufficient to achieve a high sensitivity, but it is important to design the sensor for obtaining an optimum "signal-to-background ratio" in the sense of maximizing the sensitivity in the sensing region of interest, but minimizing it in the regions of noninterest, e.g., in the cover medium above the sensing layer.

Table 1 Examples of optimum and still practical waveguide parameters for bulk refractometry, thin-layer and thick-layer sensing, for a TM_0 mode at a wavelength of 633 nm and a cover refractive index n_c=1.33

SBSR sensing layer-to-bulk volume signal ratio

Application	n_s	n_f	h_f (nm)	Sensitivity type	Sensitivity	SBSR	Penetration depth (nm)
Bulk refractometry	1.2	2.35	70	dN/dn_c	0.78	1	360
Thin-layer sensing, h_l=10 nm, n_l=1.45	1.52	2.35	200	dN/dh_l	3.0×10^{-4} nm^{-1}	0.0033	68
Thick-layer sensing, h_l=300 nm, n_l=1.40	1.2	2.35	100	dN/dn_l	0.65	34	145

We introduce here the "sensing layer-to-bulk volume signal" ratio (SBSR)

$$SBSR_{2D} \equiv S_{2D}(\partial N/\partial n_c)^{-1} = S_{2D}/S_{bulk,2D} \quad (5)$$

as a measure for the suppression of the unwanted disturbing effect of the fluctuation of the bulk volume refractive index n_c during a biosensor measurement. The ultimate aim is thus to maximize the sensitivity S_{2D} and minimize the sensitivity $S_{bulk,2D}$ at the same time. For this application, the values for $S_{bulk,2D}$ are similar, but not equal to the numerical values for S_{bulk} given in the section "Basics and bulk refractometer applications," because we take into account the presence of the sensing layer.

An additional means for enhancing background suppression is the use of reference pads [30–32] near the sensing ("signal") pads on the same chip. This on-chip referencing relies on the fact that the reference pad exhibits the nonspecific effects (e.g., bulk refractive index fluctuations, temperature), but not the specific ones (e.g., by the adsorption of the molecules to be detected).

Modeling results and discussion

Figure 5 displays numerical results for the SBSR obtained for a sensing layer with a refractive index n_l=1.45 and a thickness h_l=20 nm for the TM_0 mode at λ=633 nm. A thickness of 20 nm was chosen to be representative for very different applications with a typical sensing layer thickness range from 0 to about 40 nm. Examples are the growth of nanolayers on a chip surface, the adsorption of biomolecules to a biochemical recognition layer, and the use of intermediate layers for adapting the chemical surface properties to the effective sensing layer deposited on top.

The results show that the influence of the key parameters, i.e., film thickness h_f and the refractive indices n_f and n_s, is significantly different with respect to the sensitivity S_{2D} and the SBSR.

The results plotted in Fig. 5a,b) show that high sensitivities can be reached by choosing (1) a high film index n_f (see Fig. 5a for a substrate refractive index n_s=1.52) and (2) a low substrate index n_s (see Fig. 5b for a film index n_f=2.13). A most important design guideline can be derived from Fig. 5c,d), namely that the values of n_s and h_f have to

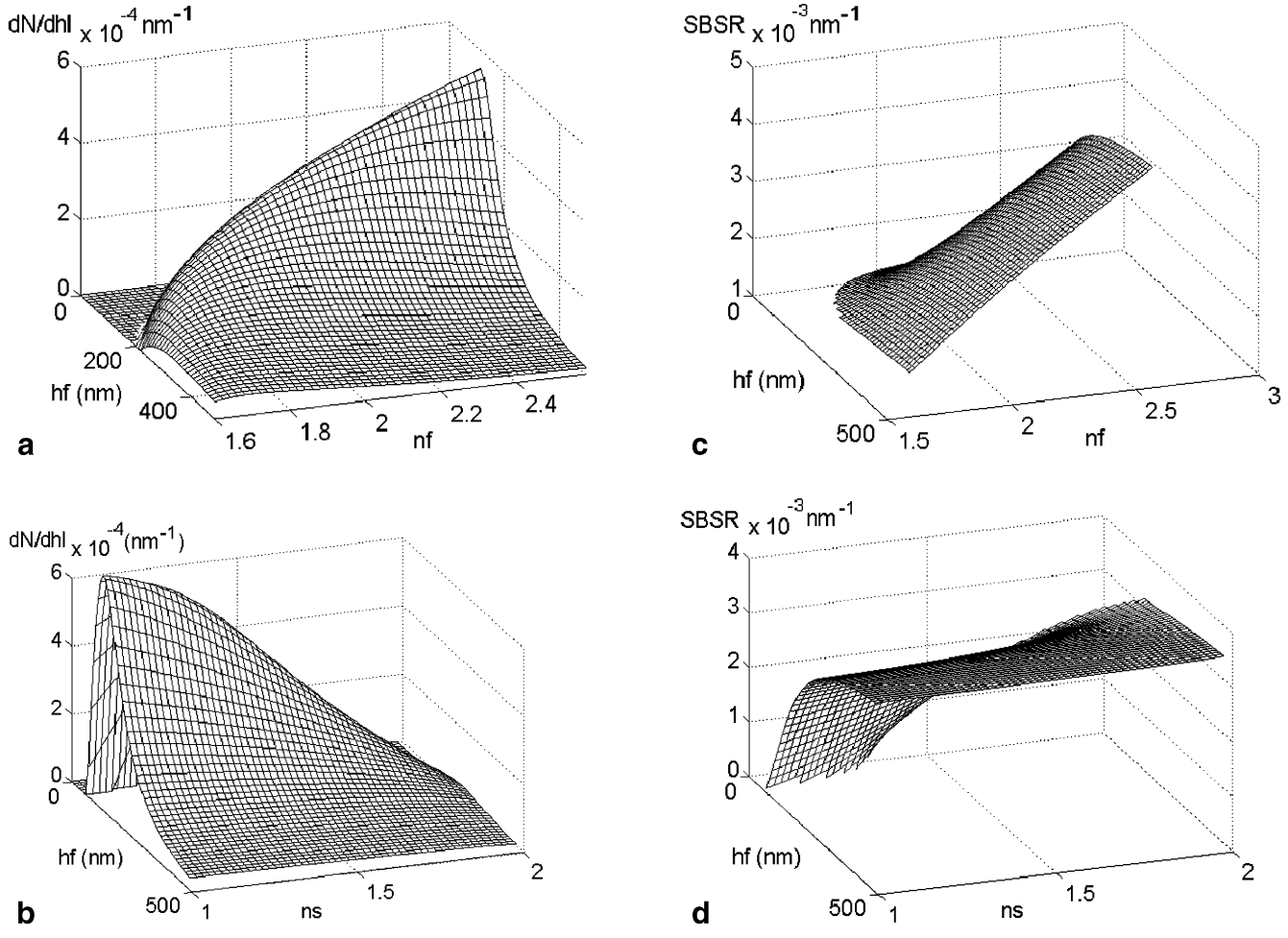

Fig. 5 Variation of the sensitivity S_{2D} (**a**, **b**) and of the sensing layer-to-bulk volume signal ratio (*SBSR*) (**c**, **d**) for the TM_0 mode as a function of film thickness and the refractive indices of film (**a**, **c**) and substrate (**b**, **d**), respectively

be balanced carefully since the SBSR tends to become small (which is unfavorable for most applications) for small substrate indices and small film thicknesses, and that the influence of n_s is higher the smaller the film thickness is chosen. Another major aspect is the importance of optimizing the film thickness h_f in all cases.

In summary, Fig. 5 shows that the highest SBSRs are obtained by choosing high film thicknesses and relatively high substrate indices, which are design rules conflicting with those for obtaining highest sensitivities.

For two representative examples, the variation of the sensitivity S_{2D} and the SBSR versus the film thickness is plotted in Fig. 6 for the TM_0 mode at a wavelength λ=633 nm and a film refractive index n_f=2.13. The results according to the solid line correspond to a Ta_2O_5 waveguide on a glass substrate [16].

In Fig. 6 the results of a "normal symmetry" waveguide (solid lines) are compared with those for a "reverse symmetry" configuration. The maximum sensitivities are 3.8×10^{-4} and 6.1×10^{-4} nm^{-1}, respectively, the optimal film thickness being about 130 nm for both configurations. While the maximum sensitivity is higher by a factor of 1.6 for the reverse symmetry configuration, the SBSR is lower, especially for smaller thicknesses (Fig. 8b).

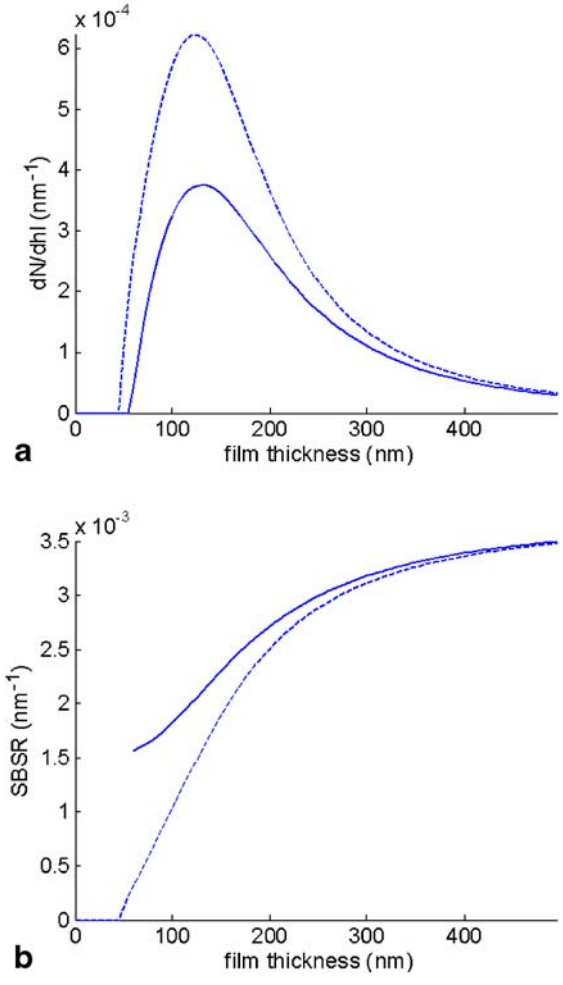

Fig. 6 Sensitivity S_{2D} (**a**) and SBSR (**b**) versus the film thickness for two waveguide configurations with refractive indices n_s=1.52 (*solid lines*) and n_s=1.20 (*dashed lines*), respectively

Hence, by means of examining Fig. 6, it is possible to tailor the sensitivity and the SBSR to the envisaged application, and also to decide if the advantages versus increased production costs will justify going to the reverse symmetry configuration. Another possibility for increasing the sensitivity is to choose a higher film refractive index, for example by choosing TiO_2 (n=2.35) instead of Ta_2O_5 (n=2.12) as waveguide material. In Table 1, an example for an optimum waveguide configuration is given, where the bias has been put on high background suppression and not on maximum sensitivity. A more extended modeling (Fig. 5) is necessary to determine which combination of film and substrate refractive index would be required to optimize sensor chip performance versus production cost.

Thick-layer sensing

Fundamentals

In this section, chip design possibilities are presented for thick-layer ("3D") sensing applications where the optical properties of a sensing matrix are modified by the presence of molecules, ions or small particles. Sensing matrices extend typically to some 100 nm from the chip's surface. Examples are hydrogel-based layers and chemo-optically sensitive membranes, also known as optrodes. An important characteristic of thick-layer sensing is the optical homogeneity of the layer. The case of optically inhomogenous layers is presented in the section "Particle sensing."

The waveguide configuration (Fig. 1c) differs from the previous one by the height of the sensing layer h_l, with a typical thickness of 30–300 nm. This is about 1 order of magnitude larger than for thin-layer sensing, and of the same order of magnitude as the penetration depth of the evanescent wave. This leads to a marked variation of the amplitude and power density in the vertical direction through the sensing layer.

A consequence of this variation is that the (matrix) sensing layer is probed with a varying local sensitivity, being higher for the portions located closer to the film and lower towards the cover medium. The aim is to get high sensitivities inside the matrix layer and low sensitivities for changes in the cover medium. This can be achieved by keeping a large fraction of the power propagated by the evanescent wave "inside" the matrix layer, resulting in very high SBSRs and a great robustness with respect to disturbances by (time-varying) properties of the sample solution (cover medium) such as turbidity, scattering and/or optical absorption [34].

The thick sensing layer is assumed to have a variable homogeneous and isotropic refractive index n_l but a constant thickness h_l. Measurements are performed by detecting the changes in the effective index N caused by changes of the measurand. Changes of the cover medium refractive index shall not influence the properties of the sensing layer.

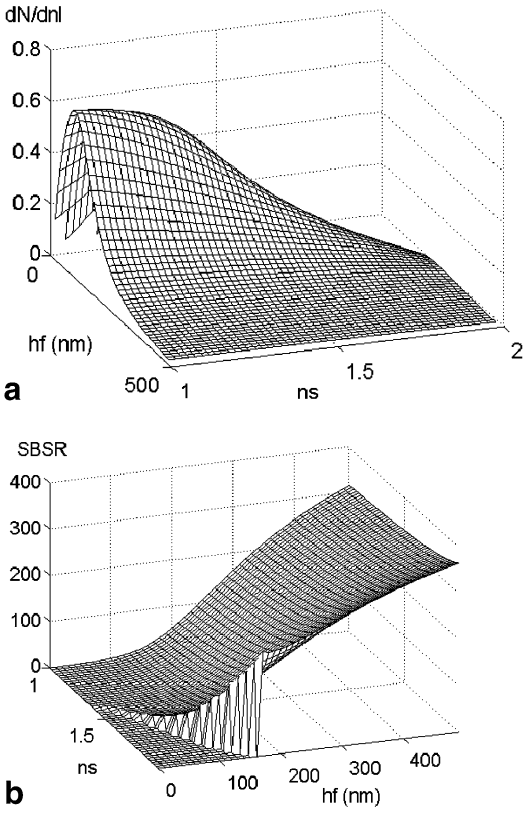

Fig. 7 Variation of the sensitivity S_{3D} (**a**) and of the SBSR (**b**) for the TM_0 mode as a function of film thickness and substrate refractive index

Hence, the sensitivity for thick-layer sensing S_{3D} is given by the partial derivative

$$S_{3D} \equiv \partial N / \partial n_l \tag{6}$$

of the effective index N by the sensing layer refractive index.

Analogously to the previous section, the SBSR

$$SBSR_{3D} \equiv S_{3D}(\partial N / \partial n_c)^{-1} = S_{3D}/S_{bulk,3D} \tag{7}$$

is a measure for the suppression of the unwanted disturbing effect of fluctuations of the bulk refractive index n_c during a measurement. For this type of application, the values for $S_{bulk,3D}$ (Eq. 3) will markedly deviate from the numerical values for S_{bulk} given in the section Basics and bulk refractometer applications" because of the presence of the thick sensing layer that changes the electromagnetic field distribution significantly. In the simplest case, the field distributions can be approximated by two evanescent waves with different penetration depth in the sensing layer and in the cover medium. However, more complex situations may arise, for example if a sensing layer is used that will form a multilayer waveguide together with the film, resulting in field distributions that are nonexponential in the sensing layer.

Modeling results and discussion

Modeling results are presented for thick-layer sensing based on a waveguide configuration with the parameter values h_l=200 nm, n_l=1.45, n_f=2.13, and λ=633 nm for the TM_0 mode. The influence of the film and substrate refractive indices is very similar to the case of bulk refractometry (Fig. 4), i.e., high sensitivities are obtained for high values of the film index (curve not shown) and for small values of the substrate index (Fig. 7a). Concerning the SBSR, very high values are obtained by choosing high values of the film index and thickness, while the influence of the substrate index is not so important (Fig. 7b).

In the case of film thicknesses greater than about 200 nm, an extremely high suppression of bulk effects can be obtained by choosing the penetration depth distinctly smaller than the matrix layer thickness, since in this case, the bulk (cover medium) is practically not "seen" by the evanescent wave that decays almost completely within the matrix layer. An example of an optimum waveguide configuration for thick-layer sensing is listed in Table 1.

An application of the thick-layer sensing approach can be found in Ref. [34], where an ion-selective (optode) membrane changed its refractive index n_l as a function of changes in the concentration of Ca^{2+} present in the cover medium. In a second example [37], an IO pH sensor was demonstrated using replicated polycarbonate TiO_2 waveguide sensor chips coated with a photopatterned hydrogel membrane.

Another possibility, not considered in this paper, is to use the matrix layer as the waveguide itself. Such a configuration, consisting of a porous Ta_2O_5 waveguide, has been successfully applied for gas (humidity) sensing [38]. Multiple modes TE_0, TM_0, TE_1, and TM_1 have been used to characterize the waveguide (ordinary and extraordinary refractive indices and thickness). In a hygrometer application, it has been demonstrated that the different modes exhibited different sensitivities.

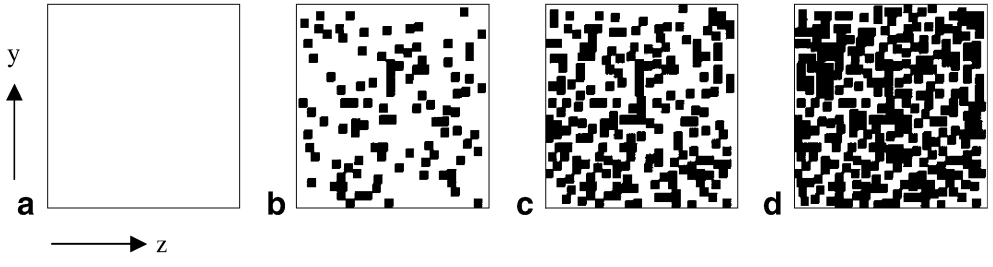

Fig. 8 Effective refractive index distribution $N(y,z)$ after deposition of **a** no cells, **b** 100 cells, **c** 200 cells, and **d** 300 cells. White domains have $N=N_1$, black domains have $N=N_2$

Particle sensing

Fundamentals

The sensor configuration considered in this section is schematically shown in Fig. 1d. It is distinctly different from the one for thick-layer sensing, because the sensing region is not defined by an optically homogeneous matrix material, but by the presence of particles near the waveguide's surface. The size of the particles is typically on the order of several hundreds of nanometers to several micrometers. In order to have a maximum signal, it is therefore in general advantageous to use geometries having a large cover field penetration depth, as has been explained in previous sections.

In order to optimize a sensor to a given measurement task and for interpretation of measurement results, appropriate modeling methods are required. If the particles are small compared with the wavelength, and appear in a large number, their presence can be modeled by applying an effective medium approach [17, 41]. Hereby, the problem is reduced to the case already discussed in the section "Thick-layer sensing," with the difference that the refractive index of the sensing layer n_l is an average between the cover refractive index n_c and the refractive index of the particle n_p. The average is calculated depending on the fraction f_p of the sensing volume occupied by the particles. It is important to note that, in general, this volume fraction is small; therefore, a change of n_c will induce a substantial change of the layer index n_l, leading to inherently small SBSR.

If the size of the particles is on the order of the wavelength and above, and if the particles appear in a small number, then effective medium theory is not applicable. Furthermore, the treatment cannot be separated anymore from the readout geometry. While interferometer-based sensors accumulate the phase-shift contributions of the individual particles, grating-coupler-based sensors are inherently sensitive to the position at which these phase shifts occur. Rigorous methods, for instance the multiple multipole method [42], rigorous coupled wave analysis [43], or the equivalent source method [44], are needed for treating such situations with high accuracy. However, these methods are in general time-consuming for both implementation and calculation. Motivated by the lack of appropriate and simple tools for modeling nonideal waveguide gratings, a novel approach was published recently [21] and developed further in Ref. [45]. It presents an efficient modeling tool for dealing with various situations of practical relevance, including nonhomogeneous waveguide thickness and/or nonuniform grating coupler properties. This approach is used in the next section to model the impact of the presence of large cells on the resonance peak of a waveguide grating.

Modeling results and discussion

For this section, it has been chosen to present modeling results related to waveguide gratings, as this resonant structure is particularly sensitive to the presence of local disturbances. Experimental observations of resonance peak shape deformations due to such disturbances have been reported in Refs. [21, 24, 25]. The results presented here

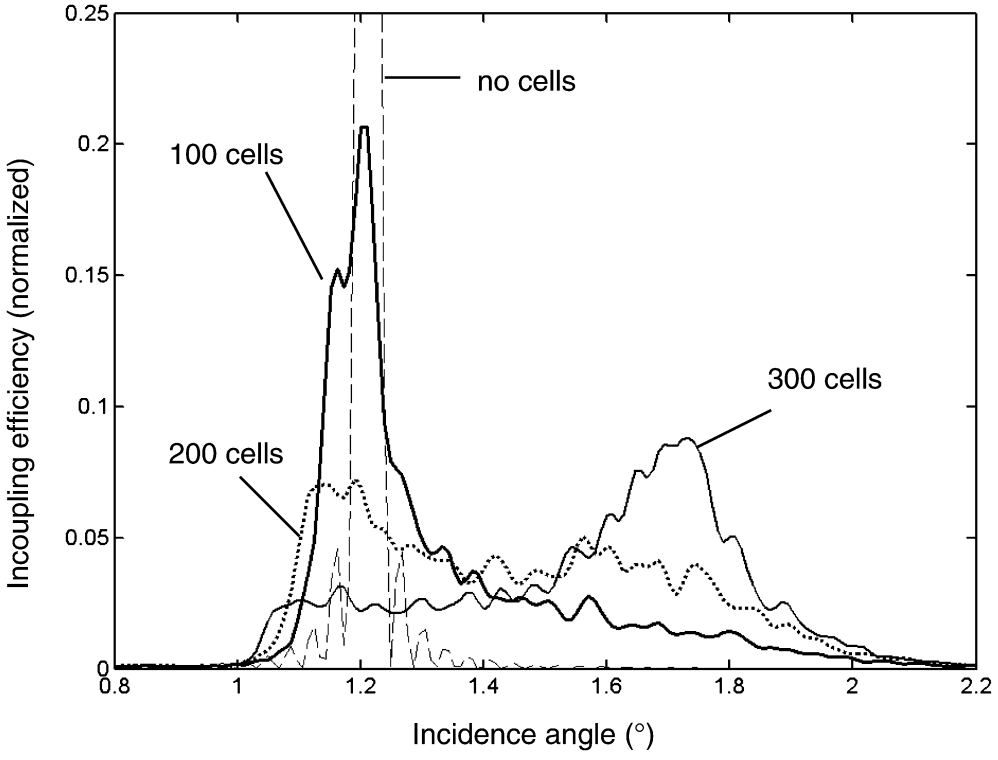

Fig. 9 Resonance line shapes corresponding to the effective refractive index distributions shown in Fig. 8a–d, respectively. The incoupling efficiency is normalized to the response of the undisturbed (no cells, $N=N_1$) waveguide

were obtained using the local interference method (LIME) [21, 45].

In the following, a situation similar to the experiments described in Ref. [25] is simulated. A reverse symmetry waveguide having a base effective refractive index N_1=1.345 is covered by large cells, modeled as quadratic regions of effective refractive index N_2=1.355 each having a surface of 45×45 μm^2. A relatively weak grating (LIME constant τ=0.999) of periodicity Λ=478 nm and situated on the waveguide is illuminated by a plane wave at different angles of incidence. The surface of the waveguide grating is 1×1 mm^2. For three stages of the particle deposition process, depicted in Fig. 8, the incoupling resonance line shape is calculated according to the scheme described in Ref. [21], namely by dividing the grating in the y-direction into slices of 9 μm, evaluating the slices individually using LIME, and summing up the results at the end for each incidence angle.

Figure 9 shows the results of the calculations for the undisturbed waveguide with N=N_1, and for a cell number of 100, 200, and 300, respectively. What can be clearly seen in the figure is an important deformation of the resonance peak. The main characteristics of the deformation, which have also been reported in the literature for the experiments, are a decrease in amplitude, and the gradual apparition of a discrete second peak. In a situation where the cell coverage is approximately 50%, the amplitude has decreased to about 5% of that in the case of an undisturbed waveguide. It should be noted that this is not due to scattering effects, since this is not included in the model. The dramatic decrease in coupling efficiency is due to a "destruction" of the resonance. Surprisingly few of these inhomogeneities are sufficient to significantly disrupt the local phase match between incident wave and waveguide mode at any incidence angle, this phase match being essential for an efficient incoupling process.

In summary, a treatment using homogenous layers having an averaged cover index of refraction is clearly not appropriate for the case of large particle detection with waveguide gratings. Such a model would simply result in a shifted peak, but neither in a deformation, nor in a significant change of the amplitude. A more sophisticated modeling is required in this case, using either rigorous tools or approximate methods such as LIME.

Conclusions

Results of a numerical study have been presented, showing that there exists a great potential and flexibility to tailor the properties of the evanescent field and the performance of IO sensor chips in general to different types of applications. This fact results from the many degrees of freedom that can be used for the IO chip design, in contrast to other technologies such as SPR sensors where the materials' properties limit the range of choices. It was investigated and demonstrated how the IO chips can not only be designed for achieving maximum sensitivity, but also to obtain an optimum "signal-to-background ratio" in the sense of maximizing the sensitivity in the sensing region of interest, but minimizing it in the regions of noninterest, for example in the bulk analyte volume.

Four distinct types of applications were considered, the first and most basic one being bulk refractometry, where the evanescent wave of a guided mode is used to measure the refractive index of the cover medium. The second application, termed thin-layer sensing, is the original driving force to develop the waveguide-based sensing approach, namely the detection of molecular species being adsorbed to a very thin recognition layer immobilized directly on the sensor chip's surface. Third, thick-layer sensing applications were treated where the task is to adapt the properties of the evanescent field to a region of interest near the surface, for instance in the case where a matrix layer of several hundred nanometers thickness is chosen to capture molecules and/or other species (e.g., ions) to be detected. Examples are chemo-optically sensitive membranes (optrodes), swellable polymers, and hydrogel-based sensing layers. Finally, particle-sensing applications were described, aiming at measuring the concentration or properties of particles in a typically micrometer-sized probing volume. Particles may range in size from nanometers to micrometers, including very large molecules or even biological cells. For these applications, a large penetration depth is advantageous. It was shown that for grating-coupler-based sensors, this kind of application can in general not be modeled using standard effective medium theory. The resonance peaks are significantly disturbed by the particles. It was demonstrated that more sophisticated tools, such as the LIME, are capable of reproducing experimentally observed peak deformations.

The results presented show that the use of high-index waveguiding films (such as Ta_2O_5 or TiO_2) provides a great flexibility to tune the properties of the sensor chips to the needs of the different types of applications. This does not only concern high sensitivity, but also the possibility to measure in a wide range of refractive indices for cover and/or intermediate layers, and to apply a wide range of different substrates and/or buffer layers, always maintaining proper waveguiding conditions. Another major advantage is that penetration depths can be achieved in an extremely wide range from well below 100 nm to arbitrarily high values. This opens up the possibility to adapt the sensor chip performance to a correspondingly wide range of applications, including those that require high background suppression.

The results will help to fully exploit the potential of IO sensor chips for present and future practical applications.

Acknowledgement We gratefully thank Guy Voirin for helpful discussions.

References

1. Homola J, Yee SS, Gauglitz G (1999) Sens Actuators B 54:3–15
2. Nagata K, Handa H (2000) (eds) Real-time analysis of biomolecular interactions: applications of Biacore. Springer, Berlin Heidelberg New York

3. Cooper MA (2002) Nat Rev 1:515–528
4. Tiefenthaler K, Lukosz W (1989) J Opt Soc Am B 6:209–220
5. Lukosz W (1991) Biosens Bioelectron 6:215–225
6. Heideman RG, Kooyman RPH, Greve J (1993) Sens Actuators B 10:209–217
7. Clerc D, Lukosz W (1997) Biosens Bioelectron 12:185–194
8. Kunz RE, Duveneck G, Ehrat M (1994) Proc SPIE 2331:2–17
9. Kunz RE (1999) In: Murphy EJ (ed) Integrated optical circuits and components. Dekker, New York, pp 335–380
10. Wiki M (2000) Integrated optical sensor micro-systems based on disposable transducers. PhD thesis no 2177, Swiss Federal Institute of Technology, Lausanne (EPFL)
11. Wiki M, Kunz RE (2000) Opt Lett 25:463–465
12. Ymeti A, Kanger JS, Wijn R, Lambeck PV, Greve J (2002) Sens Actuators B 83:1–7
13. Höök F, Rodahl M, Vörös J, Kurrat R, Böni P, Ramsden JJ, Textor M, Spencer ND, Tengvall P, Gold J, Kasemo B (2002) Colloids Surf B 24:155–170
14. Horvath R, Pedersen HC (2002) Appl Phys Lett 81:2166–2168
15. Horvath R, Pedersen HC, Skivesen N, Selmeczi D, Larsen NB (2003) Opt Lett 28:1233–1235
16. Cottier K, Wiki M, Voirin G, Gao H, Kunz RE (2003) Sens Actuators B 91:241–251
17. Kunz RE, Duebendorfer J, Morf RH (1996) Biosens Bioelectron 11:653–667
18. Parriaux O, Veldhuis GJ (1998) J Lightwave Technol 16:573–582
19. Brioude V, Parriaux O (2000) Opt Quantum Electron 32:899–908
20. Veldhuis GJ, Parriaux O, Hoekstra HJWM, Lambeck PV (2000) J Lightwave Technol 18:677–682
21. Cottier K, Kunz RE, Herzig HP (2004) Jpn J Appl Phys 43:5742–5746
22. Li PY, Lin B, Gerstenmaier J, Cunningham BT (2004) Sens Actuators B 99:6–13
23. Swann MJ, Peel LL, Carrington S, Freeman NJ (2004) Anal Biochem 329:190–198
24. Horvath R, Vörös J, Graf R, Fricsovsky G, Textor M, Lindvold LR, Spencer ND, Papp E (2001) Appl Phys B 72:441–447
25. Horvath R, Pedersen HC, Skivesen N, Selmeczi D, Larsen NB (2005) Appl Phys Lett 86:071101–071103
26. Kunz RE (1992) Proc SPIE 1587:98–113
27. Kunz RE (1993) Sens Actuators B 11:167–176
28. Zappe HP, Arnot HEG, Kunz RE (1994) Sens Mater 6:261–270
29. Kunz RE (1997) Sens Actuators B 38:13–28
30. Dübendorfer J, Kunz RE (1997) Sens Actuators B 38:116–121
31. Dübendorfer J, Kunz RE, Mader E, Duveneck GL, Ehrat M (1996) Proc SPIE 2928:90–97
32. Dübendorfer J, Kunz RE, Schürmann E, Duveneck GL, Ehrat M (1997) J Biomed Opt 2:391–400
33. Kunz RE, Gu JS (1993) In: Proceedings of the 6th European conference on integrated optics ECIO'93, Neuchâtel, Switzerland, pp 14–37
34. Freiner D, Kunz RE, Citterio D, Spichiger UE, Gale MT (1995) Sens Actuators B 29:277–285
35. Cottier K, Kunz RE, Voirin G, Wiki M (2002) Proc SPIE 4616:53–63
36. Kunz RE, Kempen LU (1994) Proc SPIE 2068:69–86
37. Dübendorfer J, Kunz RE, Jobst G, Moser I, Urban G (1998) Sens Actuators B 50:210–219
38. Kunz RE, Du CL, Edlinger J, Pulker HK, Seifert M (1991) Sens Actuators A 25:155–159
39. Nellen PM, Lukosz W (1993) Biosens Bioelectron 8:129–147
40. Lukosz W (1997) Biosens Bioelectron 12:175–184
41. Born M, Wolf E (1980) Principles of optics, 6th edn. Pergamon, New York, pp 705–708
42. Moreno E, Erni D, Hafner C, Kunz RE, Vahldieck R (2002) Opt Quantum Electron 34:1051–1069
43. Lalanne P, Morris GM (1996) J Opt Soc Am 13:779–784
44. Tishchenko AV (2000) Opt Quantum Electron 32:971–980
45. Cottier K (2004) Advanced label-free biochemical sensors based on integrated optical waveguide gratings: theory, modeling, design and characterization. PhD thesis, University of Neuchâtel, Switzerland